2019

The Structure and Stability of Cationic Metal-Benzene Clusters

Daniel P. Rabayda

The Structure and Stability of Cationic Metal-Benzene Clusters

A thesis submitted in partial fulfillment of the requirements for the degree of Master of Science at Virginia Commonwealth University.

by

Daniel Paul Rabayda

Director: Dr. Shiv N. Khanna
Commonwealth Professor
Department of Physics

Virginia Commonwealth University
Richmond, VA
May 2019

Acknowledgements

Thank you to Dr. Khanna for your guidance and wisdom that helped me to follow the right path. Thank you Dr. Reber for all of your help, guidance, and support in this research. I could not have done it without your help. Thank you Dr. Bishop for teaching me the skills I needed to perform this research. Thank you Dr. Vikas Chauhan, Dr. Dinesh Bista, Albert and Ryan for helping me in getting started and learning the fundamentals about this field. Thank you my committee members Dr. Ye and Dr. El-Shall for making time to come to my thesis defense. Thank you Vinny, David, Dillon, Josh, Gil, Swetha, and everyone else for all your help and support these past years. Thank you as well to my family and all the friends I did not mention for your support with getting me where I am today.

Abstract

We have investigated the size-dependent stability and structure of benzene, aluminum-benzene, and vanadium-benzene clusters. Motivated by gas-phase experimental studies performed by an experimental collaborator, we have used first-principle electronic structure methods to identify the structure of $Al^+(Bz)_n$, $V^+(Bz)_n$, and Bz_n clusters. Our studies reveal that cationic aluminum-benzene clusters have a magic number of 13, and that its high stability may be understood by analyzing the structure of the cluster. We also investigate the structure of vanadium-benzene clusters which have a magic number of 2. Here I examine the benzene-cation and benzene-benzene interactions that lead to these magic numbers, as well as their geometric shell structures and their formation/solvation.

Contents

Chapter 1

Introduction

Studies of the metal-benzene clusters is an extremely promising area of research as it can provide a fundamental understanding of the role of intermolecular and ion molecular interactions in governing the molecular arrangements in solutions and solids.[1, 2] Aromatic interactions are important in many materials and in biological systems motivating the need for highly accurate understanding of these weak interactions. Such an understanding is needed for a molecular insight into processes including solvation of ions by molecular clusters and ion-induced nucleation. Studies of the gas phase clusters is an important area as one can change the relative proportion of the ion-molecular and inter-molecular interactions by changing the size and the charged state.[3] One of the fundamental questions that we address is how a combination of such interactions can lead to unusually stable clusters.

For metal clusters, it is well known that small clusters exhibit "magic sizes" that appear as the peaks in the abundance spectra of the clusters generated in molecular beams. The origin of the "magic clusters" is generally understood within a model of the confined nearly free electron gas. Here, the electronic

states are grouped into shells, much in the same manner as in an atom or as in a nucleus within the nuclear shell model. When the electron count is such that the electronic shells are filled, the cluster exhibits enhanced stability and chemical inertness. These features have given rise to the concepts of superatoms as stable clusters that can mimic the chemical characteristics of atoms in the periodic table. As we will show, the mass spectra of ionized clusters composed of a metal atom surrounded by benzene molecules also exhibit sizes that are particularly stable (have higher mass intensity) compared to the neighboring sizes. Benzene is not a metal and the metal benzene clusters do not constitute a nearly free electron gas. Benzene, as we will show, do however does have a quadrupole moment. How does then the combination of metal-benzene and benzene-benzene interactions lead to unusually stable species? The present work is directed to answer some of these fundamental questions.

1.1 Background and Applications

Benzene clusters are agglomerations of 2 or more benzene molecules, and serve as an intermediate phase between that of a liquid and a gas. Benzene clusters are a particularly difficult type of cluster to study because the binding between the benzene molecules is weak, and the interaction is driven by non-covalent interactions that are difficult to evaluate using first-principles methods. An additional challenge is that the experimentally observed benzene clusters are usually ions, because neutral benzene clusters cannot be analyzed using mass spectroscopy. Force field methods for determining the structure can be done for neutral benzene clusters, however finding an accurate force field model for the ionized benzene cluster is challenging. The alternative is to use first-principles methods,

however delocalization error leads to the accuracy of these first-principles calculations to be poor. To overcome these difficulties, we have performed a combined theoretical and experimental study on metal-benzene cation clusters. The electron hole is localized on the metal ion, so first-principles methods on these systems are more accurate than in ionized plain benzene clusters. This allows us to analyze the structure, stability, and origin of stability of metal benzene clusters, and compare our results with experiments to test our hypotheses. This means that metal-benzene clusters are an ideal model system to study and analyze the difficult non-covalent interactions between benzene molecules.

A more applied reason for studying these systems include the role of metals in the breakdown of fuels. Metals may be used in a wide variety of catalysts, and the interaction between metals ions and aromatic hydrocarbons such as benzene may play an important role in their activity, coking, and breakdown. Interest in this topic is in part due to the increasing need for efficient aircraft engines that cost less fuel to run. There are several factors that contribute aircraft fuel burning efficiency, and it has been found that benzene and soot are good tracers for the inefficiency (if benzene levels drop, efficiency increases). Finding out how benzene clusters interacting with one another and with other emissions (like metals) can help to better understand what we can do to increase the fuel burning efficiency [4].

In a plain benzene cluster the benzene-benzene interactions alone are weak, but adding an aluminum or vanadium atom to that cluster we find that the benzene interacts much more strongly with the metal than with other benzenes. In the aluminum-benzene clusters we investigated, the benzene forms solvent shells around the aluminum and is much more strongly bound to the metal core than to other benzenes, and this is shown experimentally as well. This is characteristic of a charge transfer complex where for example a cationic core is a good

acceptor for surrounding benzenes to donate charge to. The benzene molecule has charge distributed unevenly giving it more negative faces than sides so that the most likely place that it would donate charge from is in fact its face which we confirm in our investigation. In vanadium-benzene clusters we found an expected sandwich covalent bond at the core of the cluster and then in larger clusters the same as aluminum where they primarily faced the center.

1.2 Magic Numbers

Magic species or their corresponding magic number is caused by a particular cluster having unusually high stability relative to other sized clusters. Depending on the experimental conditions the stability may be caused by energetic stability, geometric shell closure, electronic stability, or chemical stability. The origin of this stability may have many different causes depending on the system. We emphasize that the origin of stability in solvent clusters like water and benzene are quite different than the well-known magic numbers in metallic clusters. The identification of highly abundant, "magic" species in the mass spectra of clusters have proven valuable in nanoscience, leading to the discovery of fullerenes, and the electronic shell structures of metallic clusters. This concept originally comes from the nuclear shell model wherein certain numbers of nucleons in the nucleus have higher binding energies than other numbers of nucleons. The binding energy is largely attributed to the geometry of the nucleus and these magic numbers can be thought of as the numbers that hard spheres may find they fit closest together in. Energetically the preference of nuclei to these magic numbers can be thought of as the preference of electrons to fill or empty valence shell orbits. Magic numbers may come from a variety of different

kinds of interactions, and in this work we are most interested in the interactions between large molecules such as benzene and metals.

1.3 π Bonding and Benzene's π Orbitals

In regular covalent bonding we see valence electrons orbitals overlap so that the atoms involved with the bonding effectively share electrons. π bonding is a type of covalent bonding where the p orbitals interact with other p orbitals above and below the plane that contains the two atoms.

Benzene is a planar aromatic molecule made up of 6 carbons and 6 hydrogens forming a regular hexagon. The sides are all of the same length even though some sides are often thought of as double bonds. This is because half of the electrons forming C-C bonds are actually delocalized in torus shaped clouds above and below the faces of the benzene hexagon. These are called π orbitals since they are formed from π bonds between each of the p-orbitals of the carbon atoms. The π orbitals are in their lowest energy state when all of the p-orbitals are in phase with one another; their wave functions constructively interact giving the continuous torus shaped electron density cloud.

1.3.1 Quadrupole Moments

Quadrupole moments occur when the charge is unevenly but symmetrically distributed through a molecule. Usually monopole and dipole interactions are much stronger than quadrupole interactions so that the quadrupole moment is of little importance; this is not the case for benzene however. To explain the

quadrupole moment of benzene it is best to first visualize a simpler model, CO_2 for example.

In the linear molecule CO_2, the electrons are unevenly distributed so that the electron density is greatest around the oxygens and lowest around the carbon. This uneven charge distribution gives no additional charge so the monopole moment remains zero. There is also symmetry so that no dipole moment can come from this either. We are therefore left with a quadrupole moment where since it is the only term remaining it becomes the dominant electrostatic interaction here.

I will write the electrostatic potential out for a CO_2 molecule. I choose my axes such both oxygen atoms are along the z-axis to make calculations easier. At some observation point $\vec{r} = \vec{x} + \vec{y} + \vec{z}$ we have the Coulomb potential:

$$\Phi\left(\vec{r}\right) = \frac{1}{4\pi\,\epsilon_0}\left[-\int \frac{q\delta(x')\delta(y')\delta(z'-a)}{\left|\vec{x}+\vec{y}+\vec{z}-\vec{z'}\right|}d^3r' - \int \frac{q\delta(x')\delta(y')\delta(z'+a)}{\left|\vec{x}+\vec{y}+\vec{z}+\vec{z'}\right|}d^3r' + \int \frac{2q\delta(x')\delta(y')\delta(z')}{\left|\vec{x}+\vec{y}+\vec{z}\right|}d^3r'\right] =$$

$$= \frac{1}{4\pi\,\epsilon_0}\left[-\int \frac{q\delta(z'-a)}{\left|\vec{x}+\vec{y}+\vec{z}-\vec{z'}\right|}\,dz' - \int \frac{q\delta(z'+a)}{\left|\vec{x}+\vec{y}+\vec{z}+\vec{z'}\right|}\,dz' + \frac{2q}{\left|\vec{x}+\vec{y}+\vec{z}\right|}\right] =$$

$$= \frac{1}{4\pi\,\epsilon_0}\left[-\frac{q}{\left|\vec{x}+\vec{y}+\vec{z}-a\hat{z}\right|} - \frac{q}{\left|\vec{x}+\vec{y}+\vec{z}+a\hat{z}\right|} + \frac{2q}{\left|\vec{x}+\vec{y}+\vec{z}\right|}\right]$$

$$\Phi\left(\vec{r}\right) = \frac{q}{4\pi\,\epsilon_0}\left[\frac{2}{\sqrt{x^2+y^2+z^2}} - \frac{1}{\sqrt{x^2+y^2+(z-a)^2}} - \frac{1}{\sqrt{x^2+y^2+(z+a)^2}}\right]$$

Taking $x = 0$ and looking at just the y-z plane we have:

$$\Phi\left(\vec{r}\right) = \frac{q}{4\pi\,\epsilon_0}\left[\frac{2}{\sqrt{y^2+z^2}} - \frac{1}{\sqrt{y^2+(z-a)^2}} - \frac{1}{\sqrt{y^2+(z+a)^2}}\right]$$

We can find the electric field simply by taking the negative gradient of this potential.

$$\vec{E}\left(\vec{r}\right) = -\nabla\Phi\left(\vec{r}\right) =$$

$$= -\frac{q}{4\pi\,\epsilon_0}\Bigg[$$

$$\hat{y}\left(-\frac{2y}{(y^2+z^2)^{\frac{3}{2}}} + \frac{y}{(y^2+z^2+a^2-2a\,z)^{\frac{3}{2}}} + \frac{y}{(y^2+z^2+a^2+2a\,z)^{\frac{3}{2}}}\right) +$$

$$\hat{z}\left(-\frac{2z}{(y^2+z^2)^{\frac{3}{2}}} + \frac{z-a}{(y^2+z^2+a^2-2a\,z)^{\frac{3}{2}}} + \frac{z+a}{(y^2+z^2+a^2+2a\,z)^{\frac{3}{2}}}\right)\Bigg]$$

For comparison we also calculated the field of a CO_2 molecule in ADF.

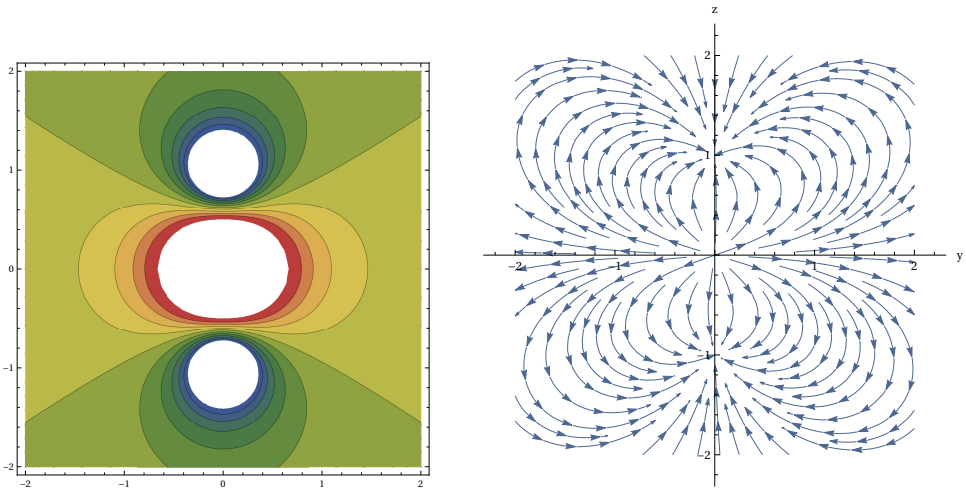

Figure 1.1: The electric potential and field of a CO_2 molecule

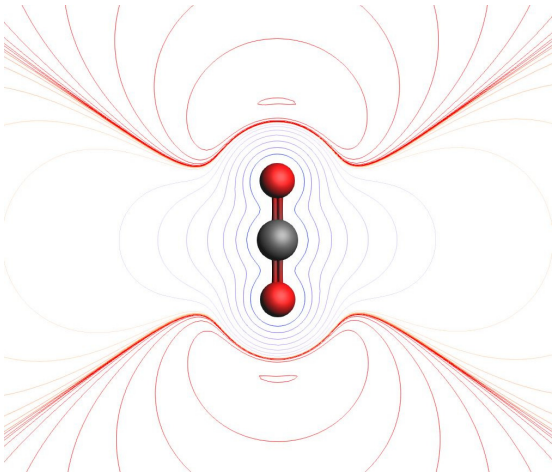

Figure 1.2: The electric potential of a CO_2 molecule as calculated using ADF.

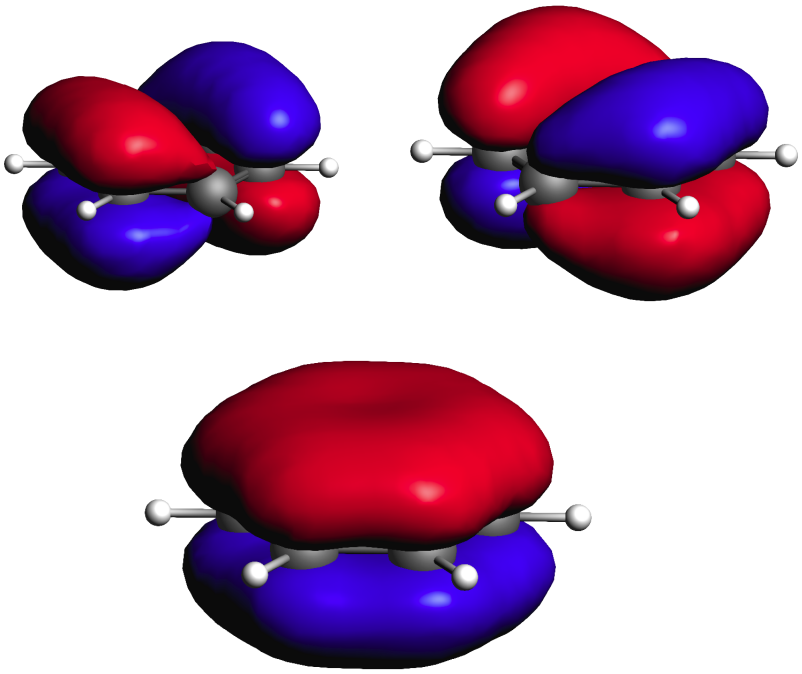

Figure 1.3: The π orbitals in in benzene. Top left and right are degenerate states.

At around 2 angstroms away we see that the potential lines are nearly identical. This is a reasonable way to model benzene's potential energy and electric field because of the similar symmetry of both systems. We can look into how this potential and field give rise to the isomers that pairs of benzene form.

The quadrupole moment of the benzene molecule comes from the π orbitals where we have two more negative faces and the outer ring of hydrogens are left with less negative charge. This forms a symmetric but uneven distribution of charge where the monopole and dipole moments go to zero leaving only a quadrupole moment. A ring of benzene's π orbitals are not quite as simple as the CO_2 molecule since benzene's π orbitals are torus shaped and they hold the greatest net negative charge.

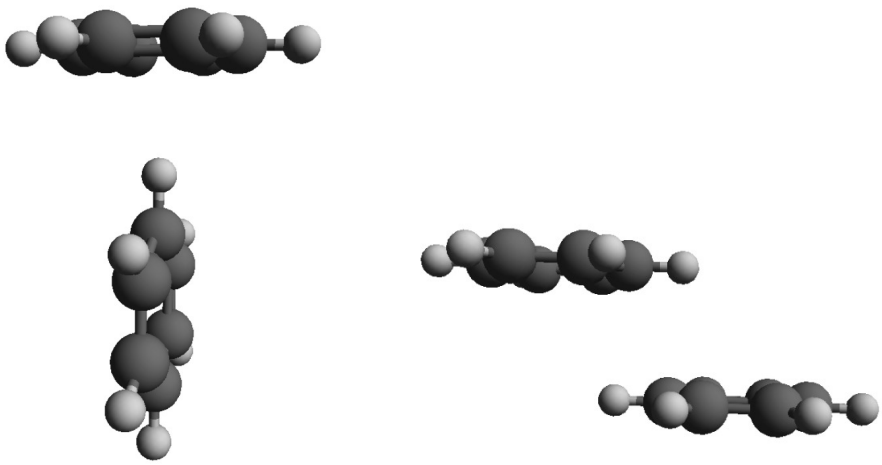

Figure 1.4: Left. Parallel displaced isomer with a biding energy of 0.12994788eV. and Right. T-shaped isomer with a binding energy of 0.12749058eV.

1.3.2 Benzene-Benzene Interactions

Benzene-benzene interactions can be thought of as quadrupole-quadrupole interactions as we have discussed. For all sizes of plain benzene clusters we see both T-shaped and parallel displaced geometries. With the aluminum and vanadium benzene clusters we see almost no T-shaped bonding, but rather that most of the benzenes face the metal ion core. This is expected for aluminum since it is positively charged so the net negative π orbitals on the benzene faces are attracted to the core so it is no mystery why they face the center in this case. There is also a π stacking benzene-benzene interaction as well as the others, however that is primarily driven by hydrophobic effects and is not of consequence for our theoretical investigations.

Sandwich structures are formed in organometallic molecules in which a transition metal atom is "sandwiched" between two benzene, or other aromatic molecules. The term sandwich comes from the geometric structure of ferrocene in which two aromatic cyclopentadiene molecules forms such a compound around

an Iron atom. [2] Since then there have been many different transition metals (like chromium, vanadium, manganese, etc.) that have been found to form this sandwich structure just as with iron. [5, 6, 7] In order for this to occur, there is covalent bonding between the metal and the benzene molecule. The $V^+(\mathrm{Bz})_2$ molecule is a particularly well known example of such a sandwich compound.

1.4 DFT

In quantum mechanics we learn about the Schrödinger equation where we take complete eigenstates to the Hamiltonian and use it to find the energy eigenvalues:

$H|\Psi\rangle = E|\Psi\rangle$

We can reverse this equation and take a good estimation for the energy of a system and find a model Hamiltonian for the ground state energy.

$(T + U + V)|\Psi\rangle = H|\Psi\rangle$

This model Hamiltonian may be operated on the system's wavefunction to get a new lower energy eigenvalue that is closer to the true ground state energy of the system. The variational method is the method by which this process is repeated to get a closer and closer approximation to the true energy of the system.

Density Functional Theory (DFT) picks up where the variational method leaves off, focused on the issue that the wavefunction is very difficult to solve exactly for a system larger than a few particles. It can be calculated by hand for a single hydrogen atom, however any larger molecule or even an atom with p, or d electron orbitals can be mathematically intense. In theory the full solution could be calculated for these large systems, however the different degrees of freedom combined with the different spins, densities, and geometries make this

calculation practically impossible currently (even for a supercomputer). We therefore apply Density Functional Theory wherein we can calculate the energies as well as the other properties simply by using electron density, and determining the exchange and correlation energy using functionals to find the converged charge density. Once the charge density is found, the forces on the atoms may be evaluated, and the lowest energy geometry may be determined.

The normal quantum physics approach to solving the ground state energy for a system is by taking a Hamiltonian and operating that on a wavefunction to get the energy eigenvalues. By taking into account every particle, interaction, and orientation of an atom we can get a total wavefunction with which to operate the Hamiltonian to operate on. DFT is the idea that this process can be reversed using the variational method to get a better Hamiltonian. The start of this came in 1927 by Enrico Fermi and Llewellyn Thomas who used the electron density dependent wave functional across the atoms in a system to minimize the energy instead of the full wavefunction. (here we call a function of another function a functional so as to distinguish it from a function of purely variables)

$$\Psi_{\vec{k}}\left(\vec{r}_1, \vec{r}_2, \ldots, \vec{r}_n\right) = \Psi_{\vec{k}}\left(n\left(\vec{r}\right)\right)$$

This is made possible because the electron density while only giving one solution at any given point contains implicit information about the system as a whole. By sacrificing some accuracy, this method made calculating the wavefunction possible for more complex systems. Not only energy, but also other characteristics of these molecules could be calculated now with fairly high accuracy simply due to the reduction of the number of variables and interactions. The probability of finding a fermion in a state Ψ_i (within a canonical ensemble) can be found by taking the Boltzmann factor of the energy in that state, and then multiplying by a normalization factor of one over the partition function (using $\beta = \frac{1}{k_B T}$).

$P_i = \frac{1}{Z_C} e^{-\beta E_i} \quad \text{where} Z_C = \sum_i e^{-\beta E_i}$

The electron density operator may therefore be written by taking a weighted sum of the Boltzmann factors with a unity operator for each state and then multiplying by that same normalization factor of one over the partition function.

$\rho = \frac{1}{Z_C} \sum_i e^{-\beta E_i} |\Psi_i\rangle\langle\Psi_i|$

This density operator can then be made into a matrix whose elements are:

$\langle x_1, x_2, \ldots, x_N | \rho | x'_1, x'_2, \ldots, x'_N \rangle = \Psi^* (x_1, x_2, \ldots, x_N) \Psi (x'_1, x'_2, \ldots, x'_N)$

We may rewrite the left side of this equation like a function:

$\rho (x_1, x_2, \ldots, x_N; x'_1, x'_2, \ldots, x'_N) = \Psi^* (x_1, x_2, \ldots, x_N) \Psi (x'_1, x'_2, \ldots, x'_N)$

Now if we take the expectation value of some observable in our system, I will call it A, we get

$\langle A \rangle = \int dx_1 \int dx_2 \ldots \int dx_N \Psi^* (x_1, x_2, \ldots, x_N) A \Psi (x_1, x_2, \ldots, x_N)$

A as an observable can be pulled out from between the states here and we will be left with

$\langle A \rangle = \int dx_1 \int dx_2 \ldots \int dx_N A \rho (x_1, x_2, \ldots, x_N; x_1, x_2, \ldots, x_N)$

And we may notice that $\rho (x_1, x_2, \ldots, x_N; x_1, x_2, \ldots, x_N)$ are the diagonal matrix components of our density matrix.

We may define the single particle density matrix in this way, where we take the integral over this density matrix with only one non-diagonal component

$\rho (x_1; x'_1) = \text{Const.} \int dx_1 \int dx_2 \ldots \int dx_N \rho (x_1, x_2, \ldots, x_N; x'_1, x_2, \ldots, x_N)$

Rewriting this in terms of the wavefunctions we have:

$\rho (x_1; x'_1) = \text{Const.} \int dx_1 \int dx_2 \ldots \int dx_N \Psi^* (x_1, x_2, \ldots, x_N) \Psi (x'_1, x_2, \ldots, x_N)$

Now we can notice that if we have direct product states giving rise to these complete states, we can find that they will contain a normalization factor of $\frac{1}{\sqrt{N}}$ each. Lets normalize the wavefunction.

$\text{Const.} \int dx_1 \int dx_2 \ldots \int dx_N \frac{1}{\sqrt{N}}$

$\phi^* (x_1) \otimes \phi^* (x_2) \otimes \ldots \otimes \phi^* (x_N) \frac{1}{\sqrt{N}} \phi (x'_1) \otimes \phi (x_2) \otimes \ldots \otimes \phi (x_N) = 1$

Distributing we are left with ones up to the state of x_1.

$\frac{\text{Const.}}{N} \int dx_1 \phi^* (x_1) \phi (x_1') = 1$

Choosing the case where $\phi (x_1')$ is $\phi (x_1)$ we are

$\frac{\text{Const.}}{N} = 1$

Const. $= N$

Thus we have found that the normalization constant here is N and we may write the single particle state as:

$\rho (x_1; x_1') = N \int dx_1 \int dx_2 \ldots \int dx_N \Psi^* (x_1, x_2, \ldots, x_N) \Psi (x_1', x_2, \ldots, x_N)$

By comparison the single particle Green's function is:

$G \left(\vec{r}, t; \vec{r}', t' \right) = G^{(0)} \left(\vec{r}, t; \vec{r}', t' \right) +$
$\int d^3x \int d^3x' \int d^3\tau \int d^3\tau' G^{(0)} \left(\vec{r}, t; \vec{x}, \tau \right) \Sigma \left(\vec{x}, \tau, \vec{x}', \tau' \right) G \left(\vec{x}', \tau'; \vec{r}', t' \right)$

Both of these can be used to reduce the number of variables in the electron density by one. Green's Function acts as a delta function when it is integrated over so that for our density operator we can use it to set two variables equal under an integration. We may alternatively or simultaneously find matrix elements from our density operator and we can ultimately take the sum of its diagonal elements to also get a density function of only one variable. We can then use these in a series to reduce the number of variables one by one to get a density function that only depends on the position it is measured at (for a ground state). This is where Hohenberg-Kohn theorem is then implemented to write the density functional in terms of this electron density.

From this density function we get a functional, and from that we can make our model Hamiltonian and ultimately a ground state energy estimate. After this the geometry of the system is manipulated slightly using force field calculations to attempt to lower the total energy of the system. The whole process is then repeated for the new system again. This cycle is run for hundreds of iterations (layered) then the converged energy is taken to be the approximate ground state

energy of the system. The approximation in this case depends on a specified degree of precision that the program is asked to reach. After the precision is high enough the resulting energy is taken then to be the ground state energy of that system.

Density Functional Theory still has some key limitations on its own which is why there have been several corrections to the energy. The greatest of these was the exchange correlation correction which gave interactions between the valence electrons and the molecules' pseudopotentials (before this it had been assumed to be a free electron gas) [8, 9]. Recently the there have been improvements in the dispersion methods accounting for van der Waals forces which are of critical importance to higher order electrostatic correction terms (i.e. dipoles, quadrupoles, etc.).

The exchange and correlation (XC) energy correction we used was GGA-PBE which stands for Generalized Gradient Approximation (specifically the one created by Perdew Burke and Ernzerhof). Generalized Gradient Approximation is an extension of LDA which is the Local Density Approximation method. In LDA the electron exchange-correlation energy is simply added to the energy of the system we had before:

$$(T + U + V + E_{\mathrm{XC}})\,|\Psi\rangle = H|\Psi\rangle$$

The dispersion correction we used was the Grimme3 BJDAMP dispersion method which similarly adds a dispersion correction energy term.

$$(T + U + V + E_{\mathrm{XC}} + E_{\mathrm{disp}})\,|\Psi\rangle = H|\Psi\rangle$$

This particular dispersion correction method is of particular importance to our system because it has the best accuracy for higher order terms necessary for multipole moments and interactions (van der Waals forces). As we have discussed benzene has only an appreciable quadrupole moment, so by implementing this particular dispersion method we were able to get correct results.

Chapter 2

Methods

Initially we had been sent experimental data from our collaborators Professor Zhixun Luo and co-workers who found that aluminum-benzene and vanadium-benzene clusters appeared to have magic numbers. Using a custom mass spectrometer they found higher counts corresponding to specific numbers of benzenes for each. It appeared that $Al^+(Bz)_{13}$ was magic as well as the confirmation of a well known stable sandwich cluster $V^+(Bz)_2$.[6] (see fig. 2.1)

We started out trying to get the results others had gotten for plain benzene clusters.[1-3] To get binding energies we first used ADF to find the lowest energy structure for each cluster. After this we took the energy of the n-1 cluster and added the energy of a single benzene to it, then took the difference between that and the n'th benzene's total energy. This gave us the binding energy for the plain benzene clusters where we found the similar results as previous studies for the plain benzene clusters, with Bz_{13} being a magic number for the plain cluster. After this we began trying aluminum cations and one benzene on it. We found that there were several different ways the aluminum could alter the planar structure of benzene, and accounted this to benzene's bonding and an-

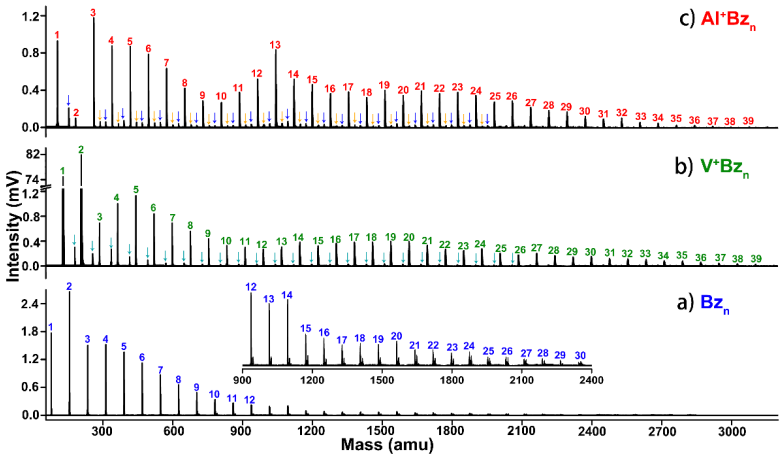

Figure 2.1: Mass spectrometer data received from our collaborators Professor Zhixun Luo and co-workers

tibonding molecular orbitals (because they matched the geometries of what we saw). Among these the planar structure remained the lowest energy geometry so we continued with higher numbers of benzenes arranged around the aluminum. Once we got to around 6 benzenes it became clear that these geometries were getting too complex to guess correctly on our own so we began using the molecular modeling software Tinker to get force field corrections to the geometries before running them in ADF.[10] Tinker does not have an aluminum cation in any of its parameter files, but we found the closest comparison we could find was a calcium +2 cation (number 354 in oplsaa.prm). This returned the same structures as we had been getting with ADF for 1 to 7 benzenes so we ran force field approximations with it many times for each larger structure. We found several geometries to be common for each structure so we ran those with ADF and found that they in fact had lower energies than the less common geometries, except for in 12 13 and 14. In these we found that there were 3 outer benzenes that ADF kept having trouble finding a place for in the geometry, until we found the current lowest structure for 13. This was the lowest energy geometry by far,

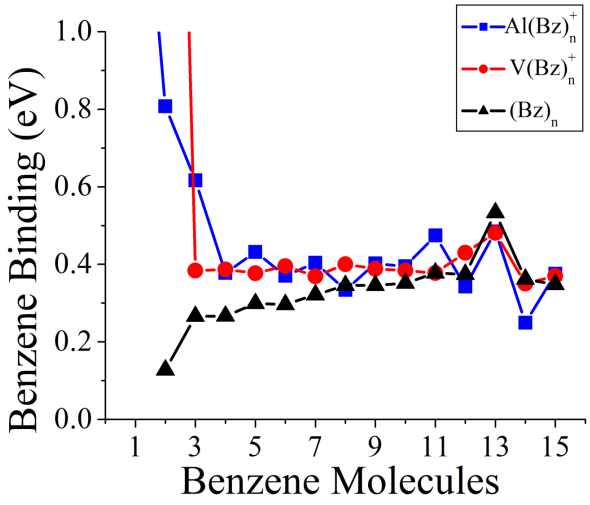

Figure 2.2: Binding energies scaled to see magic numbers

but we had not have gotten it from just force field corrections since the 3 outer benzenes are all T-bonded to one another. From this two conclusions may be drawn, one that Tinker was not giving us the true lowest energy structures for any of the trials, or two that the structure of 13 was unique. We tried the same process with several of the other structures, however none were affected except 12 and 14. Since the inner "layers" of the 13 structure were similar looking to the smaller structures we came up with a way to categorize these "layers" of benzenes. We had found that the first layer (immediately surrounding the aluminum cation) was always either 3 or 4 benzenes facing it. The 3 were wrapped around and we called this the ring isomer whereas the 4 had a lopsided ring of 3 with a 4th on the free side, we called this a single capped isomer. We found the next layer for a ring base had two capping benzenes that were often tilted away from facing the aluminum (see fig. 2.3). The binding energies of the aluminum-benzene clusters peaked at 13 which after careful reconsideration and multiple different trial structures we confirmed this result (see fig. 2.2).

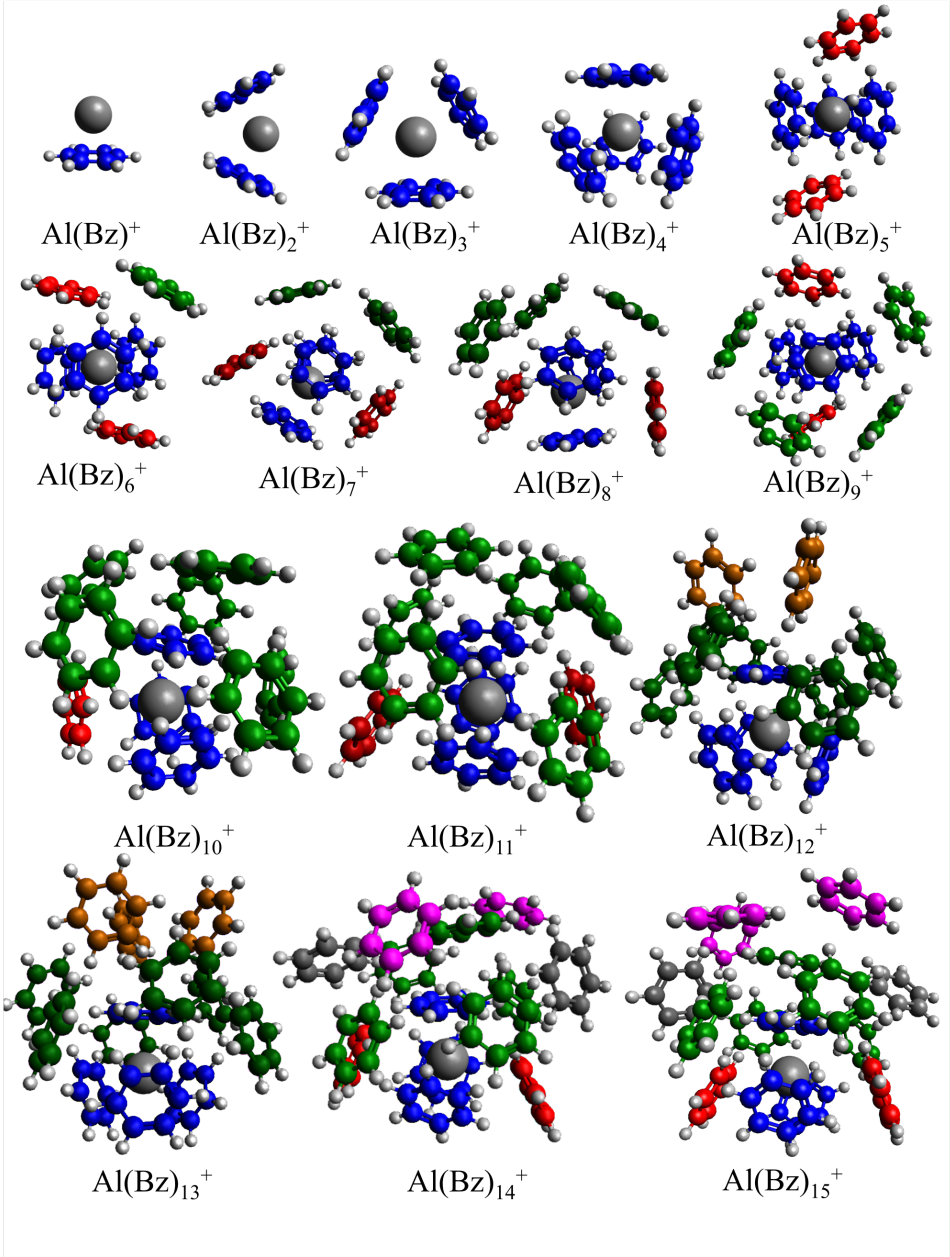

Figure 2.3: Aluminum-benzene clusters

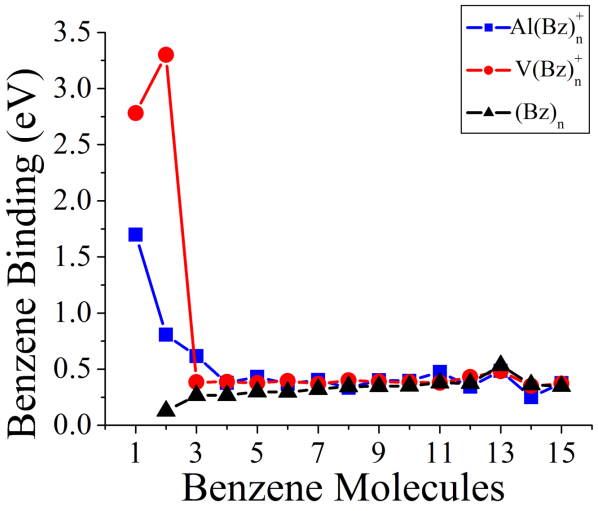

Figure 2.4: Binding energies scaled to see vanadium-benzene's peak at 2

For vanadium-benzene clusters, we followed the same method as with aluminum but in this case we expected a sandwich structure base. We found that our data agreed with previous papers.[5, 6] For our method of finding larger structures we used Tinker for force field optimization again but with vanadium we used a magnesium cation instead which gave us sandwich structure bases as expected (see fig. 2.5). As for layering, benzene did not appear to prefer discrete angles as they formed around the sandwich complex, however their distances from the center were discrete. The binding energies were similar, except for the disproportionately large binding energy of the sandwich complex (see fig. 2.4).

In addition to the binding energies we also found the ionization potentials for both aluminum and vanadium each with their neutral and +2 cation structures. To do this we first used ADF to get the lowest energy structures of neutral and +2 cation clusters. Once we obtained these we took the dif-

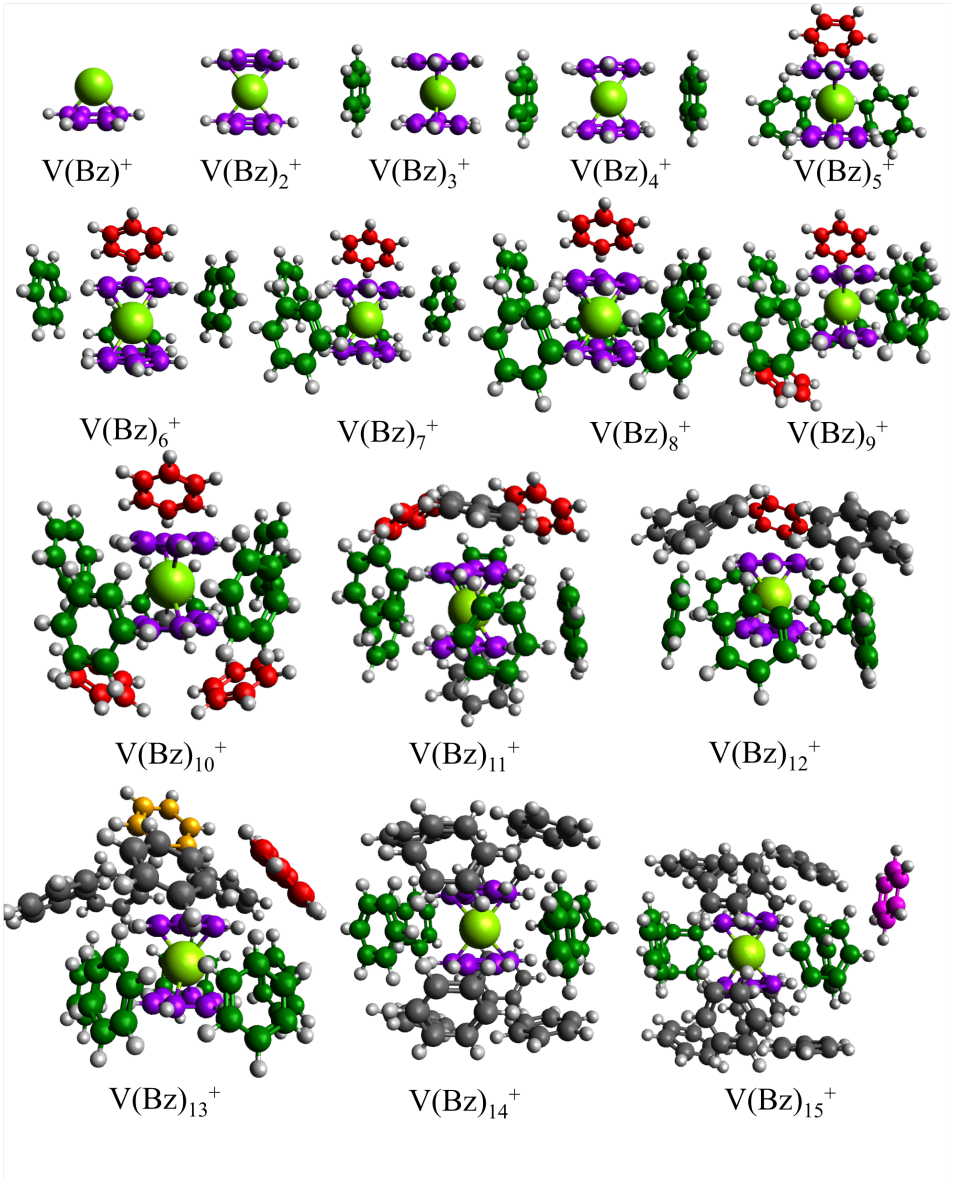

Figure 2.5: Vanadium-benzene clusters

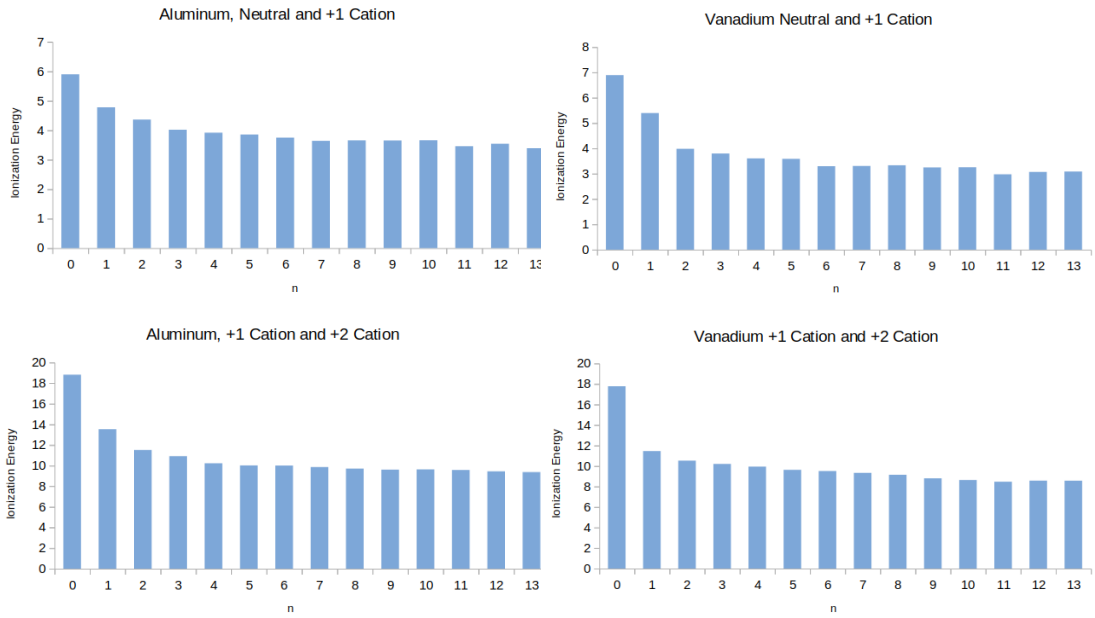

Figure 2.6: Ionization energies

ference between the ground state energies of the neutrals and +1 cations as well as that between the +1 cations and +2 cations (see fig. 2.2 and 2.4) We see that in all cases the ionization potential decreases as n increases. We also looked into the Homo-Lumo gap which is fairly consistent across all n for both aluminum-benzene and vanadium-benzene clusters.

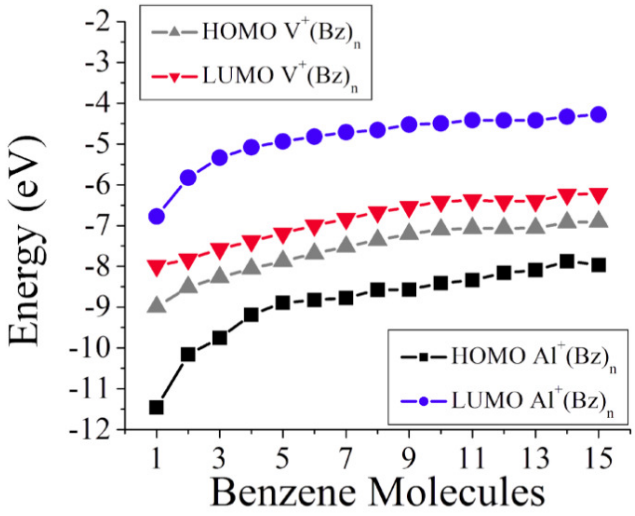

Figure 2.7: Homo-Lumo energies

Chapter 3

Results and Discussion

We confirmed in our study that for clusters of just benzene, 13 is a magic number. We also have found that 13 is a magic number in aluminum-benzene and vanadium-benzene clusters as well. The aluminum-benzene clusters are of particular interest since they do not have a sandwich structure in the core of the clusters. There are instead 3 to 4 benzenes that form a solvent shell around the aluminum, which are surrounded by another shell of benzenes. The distance from the aluminum to the center of each benzene directly surrounding it is around $2.75\mathring{A}$ while for vanadium that same distance is $1.72\mathring{A}$. In vanadium-benzene the sandwich structure is a covalent bond, however in aluminum-benzene this is not close enough for a covalent bond and instead the interactions we see appear to be that of a charge transfer complex. We see that if we compare the binding energies of plain benzenes with the binding energies of benzene aluminum we see that aluminum's is greater for the smaller structures (see in fig 2.2). Since these binding energies are relative to each system we can't just take this at face value, but instead it is important to also look at the geometry of the benzene with itself.

We found more and more that the benzene molecules would form in specific ways around the core metal atom (especially apparent in Vanadium), so we came up with a way of classifying these common structures by the use of what we call a geometric basin plot. On this we have plotted on one axis the angle that each benzene face is tilted away from the central metal atom, and on the other axis their distance from the central metal atom. In this we have assumed that the benzene molecules are each more or less planar and that the area vector of that plane can be determined from the cross product between two vectors in that plane; we called this $\vec{u}_i$. We took the average positions of each atom in the benzene to be the central position, and comparing that position with the position of the central metal gave us our radial vector $\vec{r}_i$. Using these two vectors we could then easily find the angle between them by taking their dot product and their lengths ($\vec{r}_i \cdot \vec{u}_i = \left|\vec{r}_i\right| |\vec{u}_i| \cos\theta$). This alone could produce several different results for example if they pointed in exact opposite directions then we would see 180° instead of 0° so for angles greater than 90° we just subtracted 90°. We have plotted the radial vector's length, versus the angle we found between the radial and normal area vectors for each benzene in each system (see fig. 3.1).

This geometric basin plot gives us a way of displaying a key point to our results, that the number of benzenes around the metal form into solvent shells. It also shows that these shells each affect the geometry of the innermost "shell" of benzene molecules in aluminum-benzene clusters. In vanadium-benzene clusters there is no effect on the sandwich structure by larger solvent shells. We also notice that the angles are much more dispersed in vanadium than in aluminum which plainly means that the solvent shells that form around aluminum prefer specific angles while the vanadium cluster's benzenes do not. This finding means that the benzene-benzene interactions must play some role in the formation of

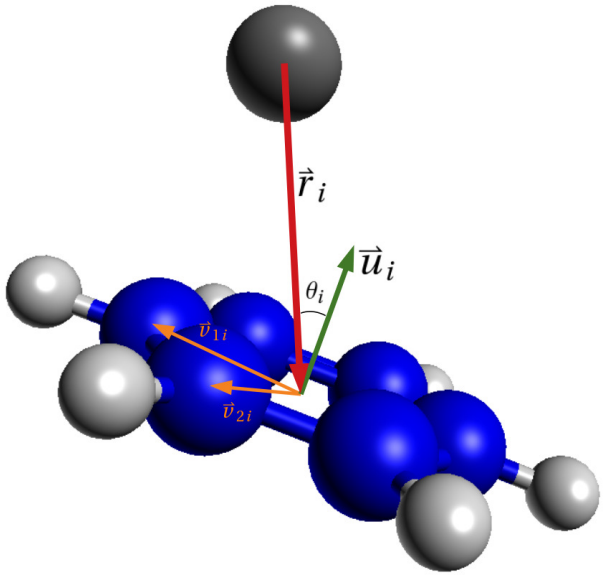

Figure 3.1: Definitions of vectors used in calculation of the angle θ_i for each benzene in a given cluster

the aluminum-benzene solvent shells.

To get the benzene-benzene basin plots we again found the radial vector to the center of each benzene and found their area normal vectors again. This time however, we compared pairs of benzenes in each geometry, one centered at $\vec{r}_i$ and one centered at $\vec{r}_j$. We found a vector going from the center of one to the center of the other and called this $\vec{r}_{ij} = \vec{r}_i - \vec{r}_j$. After this we found the normal area vector of each benzene using the same process as before, then calculated the angle that each of these made with $\vec{r}_{ij}$. We were then able to plot these angles against the length of the distance between benzenes r_{ij} (see fig. 3.5). We also found the angle between the normal area vectors themselves so that we could then categorize which pairs were truly parallel displaced isomers and which were false positives (an example of one of these may be seen in fig. 3.4). Looking at the normal area vectors in fig. 3.4 we see that they are about 90° apart while in a true parallel displaced we would have around 0°. This is the

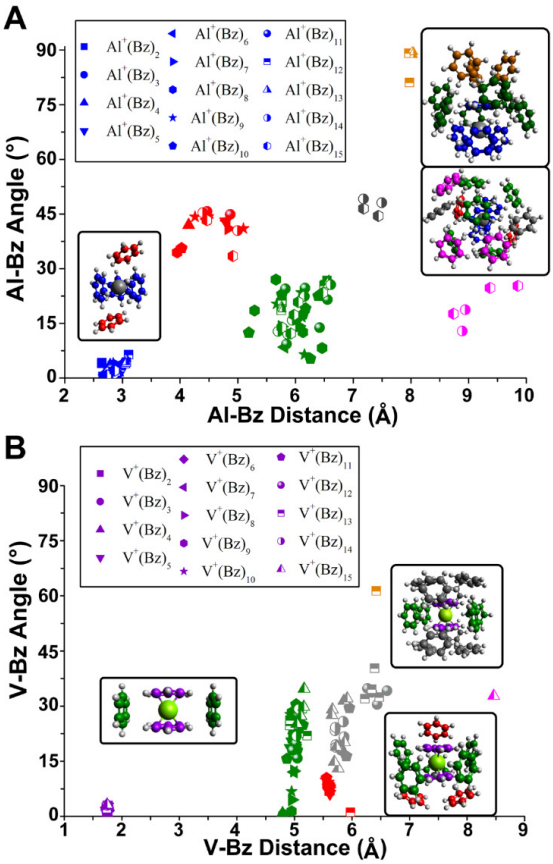

Figure 3.2: Geometric basin plot of each angle θ_i against the distance to the center r_i

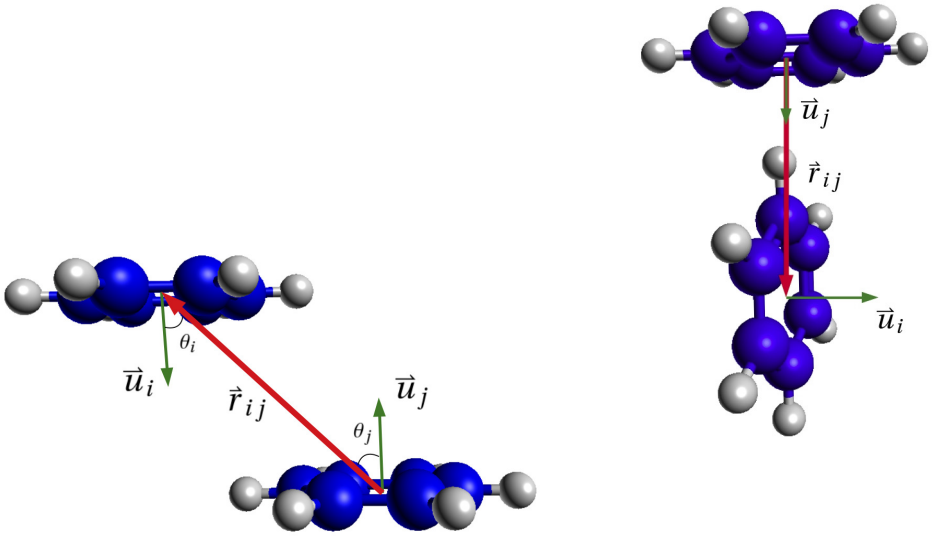

Figure 3.3: T and parallel displaced isomers with the vectors we used to find the angles θ_i and θ_j for each pair of benzenes in a given cluster

second method of categorization. Although important, the angle plots were difficult to pick out T and parallel displaced isomers from visually so we found a new value that is the difference of the two angles in a given interaction pair. The way to interpret these is that the angle difference should be around 90° for the T isomers, and 0° for the parallel displaced (along with the additional constraints against the false positives). Since the basin plots did not show all of this data as cleanly, we took a smooth density histogram for fig. 3.6 where we plotted this angle difference against r_{ij}.

The density plots show that the T isomer is definitely dominant in the clusters overall, however this may have some influence based on the tendency to face the center of the cluster. What can be said of the left graphs is that there are discrete basins that the benzenes form which supports the claim that there are solvent shells forming around the metal core. Notice in the aluminum-benzene all data plot that near about $5\mathring{A}$ there is a high density near an angle difference of zero. This is showing that the closest benzenes in the structure all

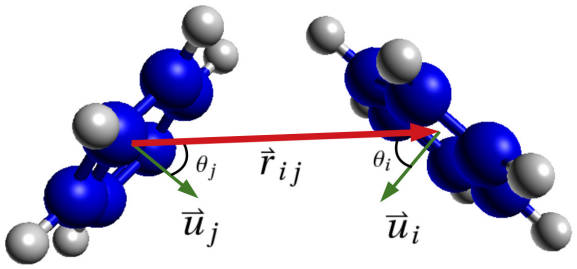

Figure 3.4: A false parallel displaced isomer by our first method of categorization. This is accounted for by our second method.

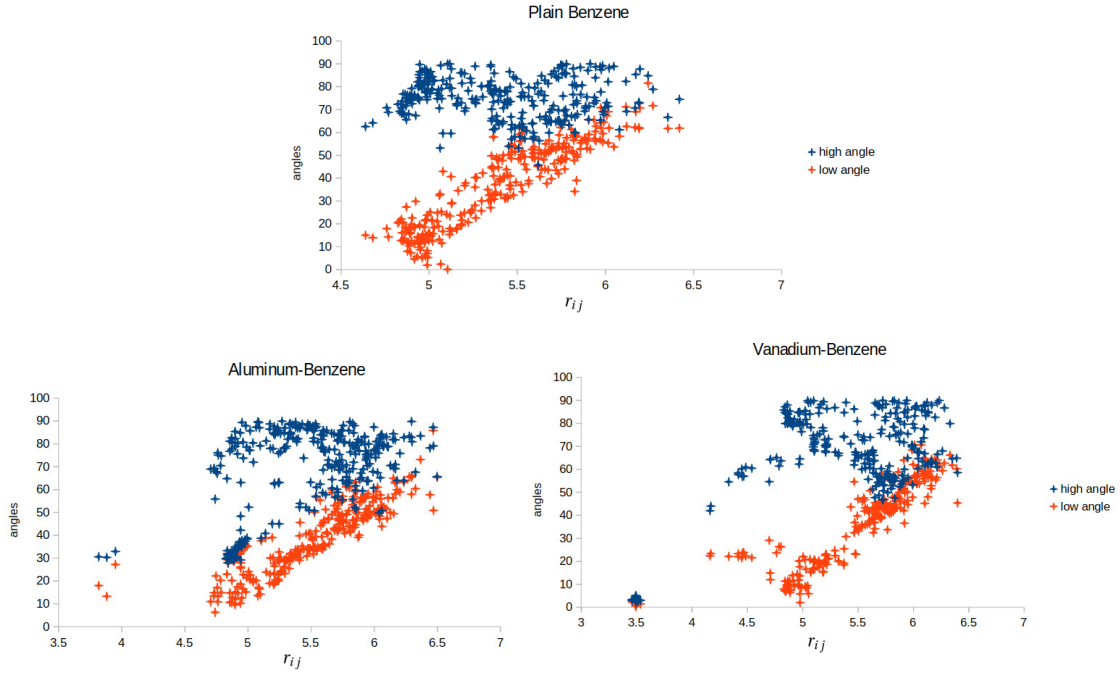

Figure 3.5: Basin plots of the angles θ_i and θ_j against the distance between the pair of benzenes r_{ij}

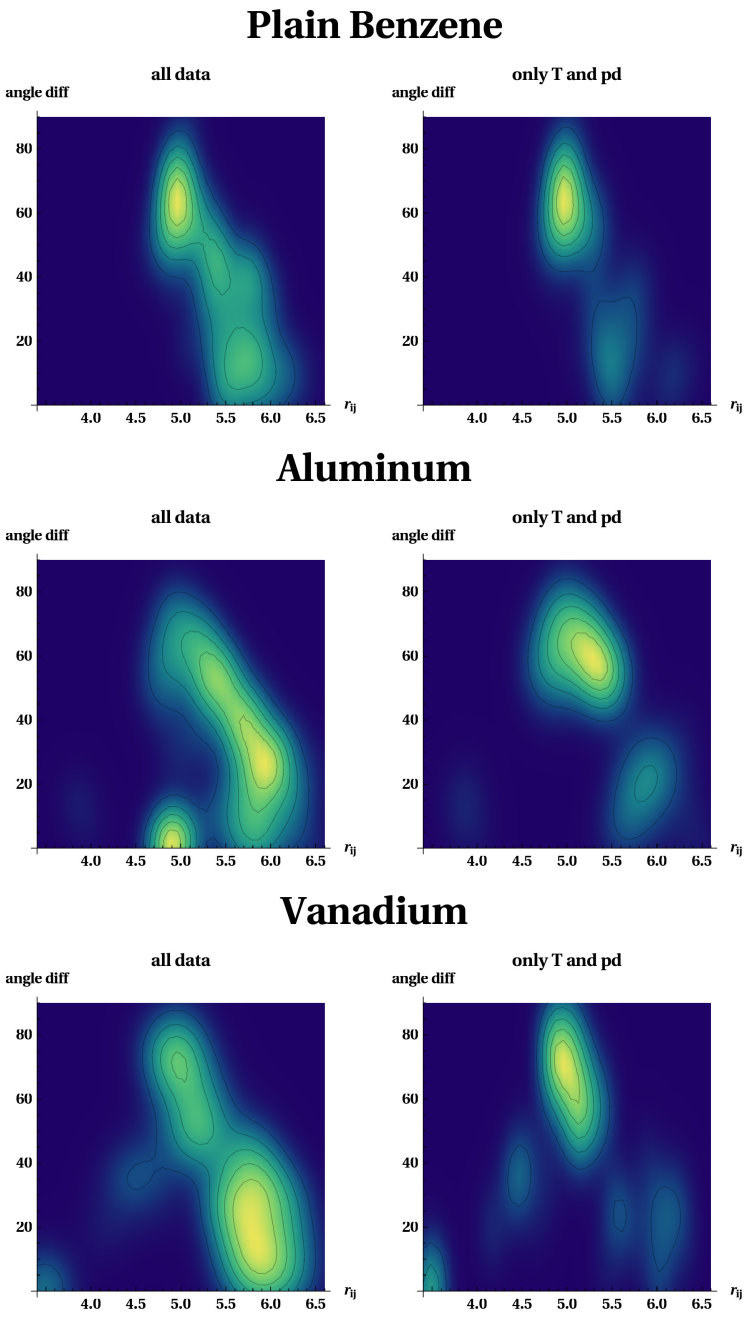

Figure 3.6: Smooth density histograms of the difference in the two angles $\theta_{i\,j}$ against the distance between the pair of benzenes $r_{i\,j}$

have nearly zero angle difference. Looking at the plot of only T and pd isomers, we see that these vanish indicating that while the angles they make with their common distance vector are similar, their area vectors still point in different directions. This is our "fake" parallel displaced isomer as seen in fig. 3.4 and with so many of these in aluminum near one another we may guess that these are the ones surrounding the aluminum core. After checking, we confirmed that these are actually the first solvent shell that forms around the aluminum.

We also modified our method above to find just the distance between each pair of benzenes across all clusters. We found that these distances were sectioned off into relatively gaussian distributions (see fig. 3.7). This helps support the claim that the benzenes are forming discrete geometric shells around the core. The fact that the first peak and second peak have a clear separation means that we can investigate all of those below around 6.7$\mathring{A}$ for nearest-neighbor interactions between benzenes.

From the distributions of the The amounts by which the counts of the lowest peak increase for each cluster size can tell us how densely packed our clusters are. To get these we first found the total number of benzenes within a range of 0-6.7$\mathring{A}$ for each cluster, then found the change in that total from the n-1 cluster to the n cluster. For comparison the change in total number of possible interactions would be a linear trend; starting at 3 it would be 2, at 4 would be 3 and so on. We plotted these differences in fig. 3.8 and found that the overall changes in density of the clusters strongly resembles the binding energies of those clusters. This gives us another way of showing that 13 is a magic number in each of these clusters.

With this we can reason that clusters who have more benzenes that are closer to one another and therefore have greater density. With a greater density here we see a direct correlation to binding energy of our system. The peak

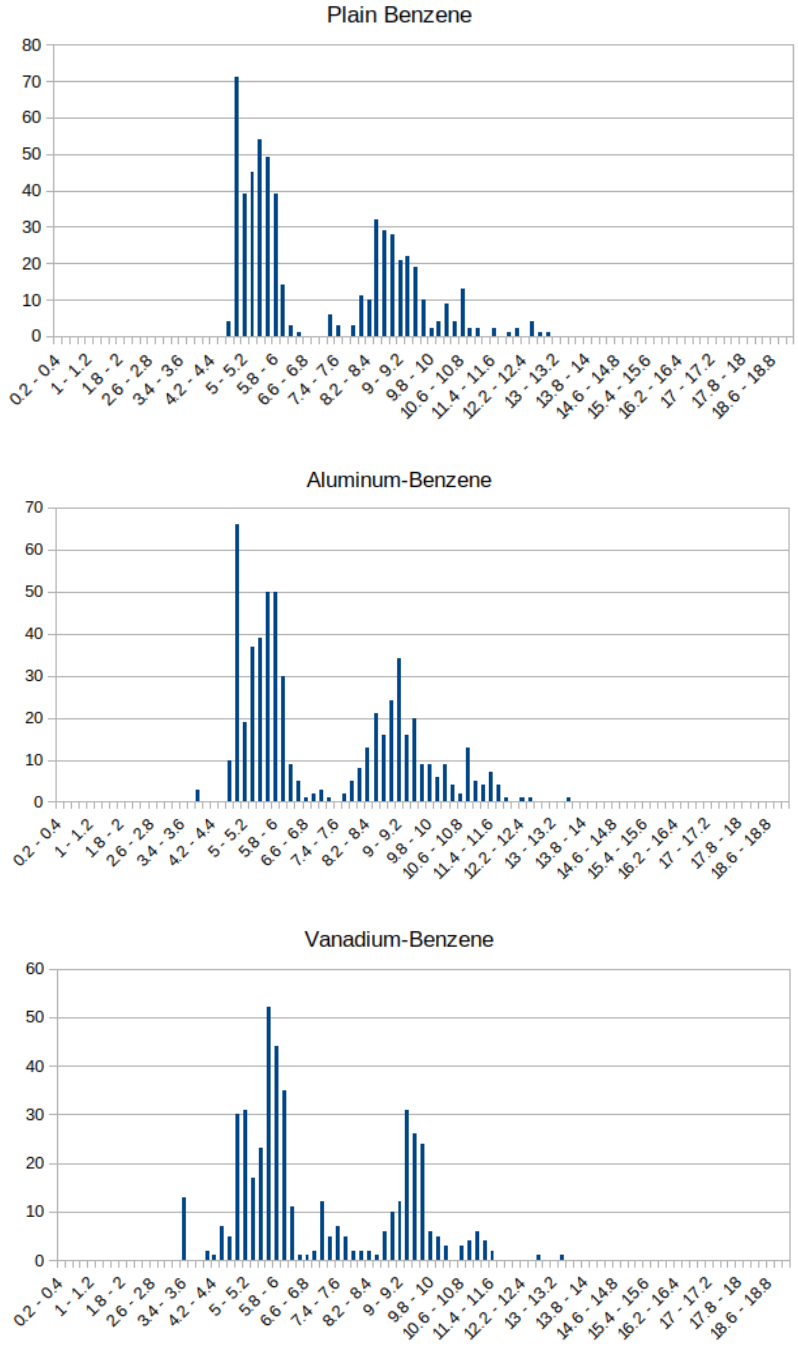

Figure 3.7: Histograms of all the r_{ij} for each cluster type.

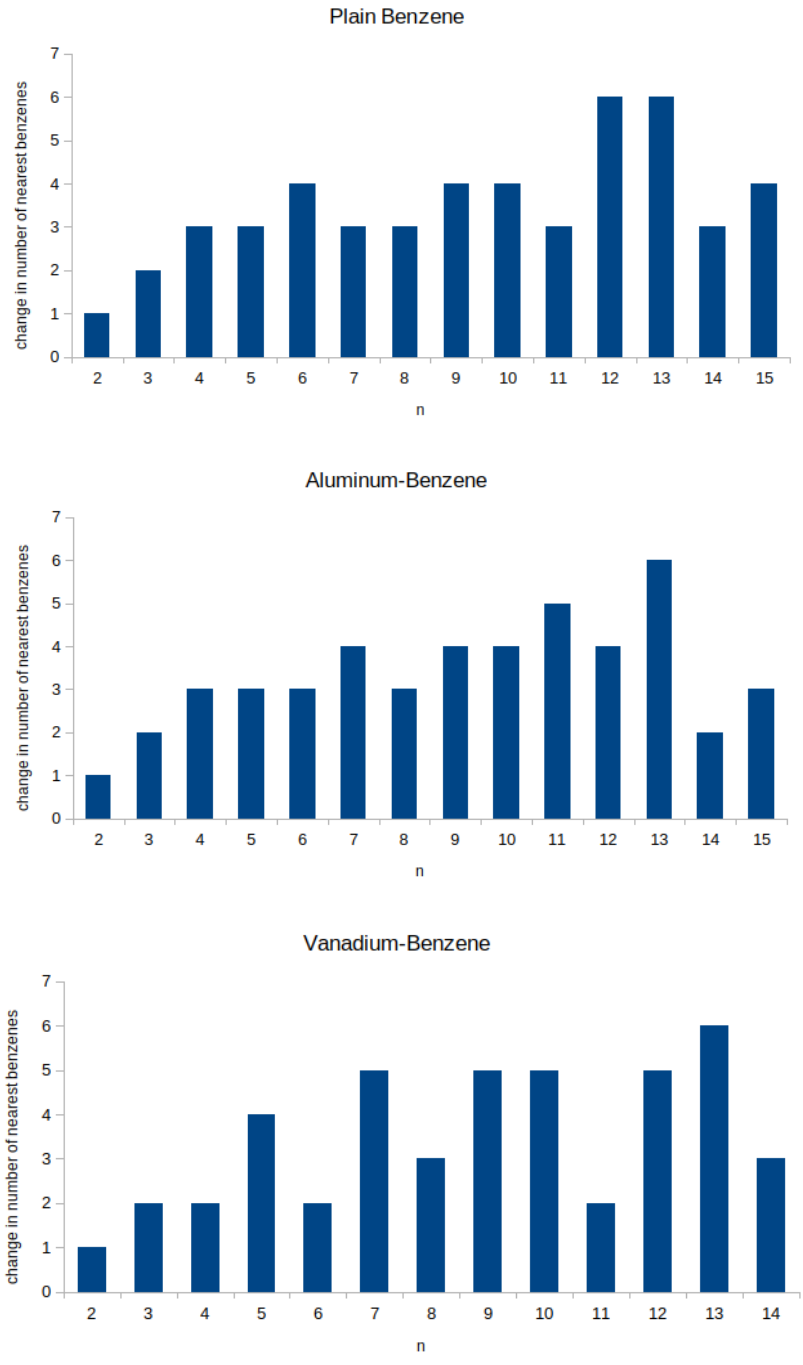

Figure 3.8: The changes in nearest benzenes against cluster size

around 13 is common in each which is no coincidence if the binding energy is strongest in 13, then the packing density should also be at a local maximum. It is also worth mentioning that this not only resembles the peaks at 13 but also the smaller peak at 11 in aluminum-benzene clusters and several other characteristics of the binding energy graphs as well.

Chapter 4

Conclusion

We have confirmed experimental findings, that 13 is a magic number in aluminum-benzene clusters as well as in vanadium-benzene clusters. There are solvent shells that are apparent in both sets of clusters which give rise to these highly stable species. In aluminum-benzene clusters each benzene is only interacting from a distance with the aluminum and the system is like that of a charge transfer complex. In vanadium-benzene clusters the vanadium center forms covalent bonds with the two sandwich benzenes directly surrounding it. The rest of the benzenes form around this sandwich structure all facing the sandwich. In general conclusions cannot be drawn from only this because the geometry must be taken into account for each cluster, however some general conclusions may be drawn still. For example, it appears that in the sandwich structure the vanadium cation remains overall positive in smaller clusters to make the other benzenes that form around it face toward it. In larger clusters however, we see that the preference is not actually towards the center but towards the hydrogens. This means that the sandwich structure must quench the vanadium's field appreciably so that the quadrupole-quadrupole interactions of

the benzenes has a visible effect still.

These geometries ultimately give rise to the magic numbers appearing in the binding energies for each set of clusters. The link between the geometry of the system and the binding energies can be best described by the density of the benzenes in each cluster size. This is found by the difference in nearest benzene count between each cluster size and has been shown to closely resemble the binding energies. Even though the solvent shells do not form the same way for aluminum and vanadium, these magic numbers in the geometry indicates that there is something that is even more fundamental about this interaction. The study of metal benzene clusters can help us understand the fundamental interactions between benzene molecules in a way that combines experiment and theory.

Bibliography

[1] Hiroshi Takeuchi. "Structural Features of Small Benzene Clusters (C6H6)n (n $\leq$ 30) As Investigated with the All-Atom OPLS Potential". In: *The Journal of Physical Chemistry A* 116.41 (2012). PMID: 22994397, pp. 10172–10181. DOI: 10.1021/jp305965r. eprint: https://doi.org/10.1021/jp305965r. URL: https://doi.org/10.1021/jp305965r.

[2] J. D. Dunitz, L. E. Orgel, and A. Rich. "The crystal structure of ferrocene". In: *Acta Crystallographica* 9.4 (Apr. 1956), pp. 373–375. DOI: 10.1107/S0365110X56001091. URL: https://doi.org/10.1107/S0365110X56001091.

[3] Mark J. Rusyniak et al. "Gas-Phase Ion Mobilities and Structures of Benzene Cluster Cations (C6H6)n+, n = 2-6". In: *Journal of the American Chemical Society* 125.39 (2003). PMID: 14505422, pp. 12001–12013. DOI: 10.1021/ja035504m. eprint: https://doi.org/10.1021/ja035504m. URL: https://doi.org/10.1021/ja035504m.

[4] Michael T. Timko et al. "Composition and Sources of the Organic Particle Emissions from Aircraft Engines". In: *Aerosol Science and Technology* 48.1 (2014), pp. 61–73. DOI: 10.1080/02786826.2013.857758. eprint: https://doi.org/10.1080/02786826.2013.857758. URL: https://doi.org/10.1080/02786826.2013.857758.

[5] Christoph Elschenbroich et al. "Metal π Complexes of Benzene Derivatives. Germanium in the Periphery of Bis(benzene)vanadium and Bis(benzene)chromium. Synthesis and Structure of New Heterametallocyclophanes,1". In: *Organometallics* 16.21 (1997), pp. 4589–4596. DOI: 10.1021/om970249y. eprint: https://doi.org/10.1021/om970249y. URL: https://doi.org/10.1021/om970249y.

[6] Tsugunosuke Masubuchi, Takeshi Iwasa, and Atsushi Nakajima. "Multiple-decker and ring sandwich formation of manganese–benzene organometallic cluster anions: MnnBzn- (n = 1-5 and 18)". In: *Phys. Chem. Chem. Phys.* 18 (37 2016), pp. 26049–26056. DOI: 10.1039/C6CP05380G. URL: http://dx.doi.org/10.1039/C6CP05380G.

[7] Kyo-Won Choi et al. "Clustering Dynamics of the MetalBenzene Sandwich Complex: The Role of Microscopic Structure of the Solute In the Bis(η6-benzene)chromium·Arn Clusters (n = 1-15)". In: *The Journal of Physical Chemistry A* 112.31 (2008). PMID: 18620373, pp. 7125–7127. DOI: 10.1021/jp804601f. eprint: https://doi.org/10.1021/jp804601f. URL: https://doi.org/10.1021/jp804601f.

[8] "The Calculation of Atomic Fields". In: *Mathematical Proceedings of the Cambridge Philosophical Society* 23 (Jan. 2008), pp. 542–546. DOI: 10.1017/S0305004100011683.

[9] "Statistical method to determine some properties of atoms". In: *Rendiconti Lincei. Scienze Fisiche e Naturali* 22 (Dec. 2011), pp. 283–314.

[10] Joshua Rackers et al. "Tinker 8: Software Tools for Molecular Design". In: *Journal of Chemical Theory and Computation* 14 (Sept. 2018), pp. 5273–5289. DOI: 10.1021/acs.jctc.8b00529.

[11] Dwaipayan Chakrabarti et al. "A survey of the potential energy surface for the (benzene)13 cluster". In: *Phys. Chem. Chem. Phys.* 13 (48 2011), pp. 21362–21366. DOI: 10.1039/C1CP22220A. URL: http://dx.doi.org/10.1039/C1CP22220A.

[12] Marcey L Waters. In: *Current Opinion in Chemical Biology* 6.6 (2002), pp. 736–741. ISSN: 1367-5931. DOI: https://doi.org/10.1016/S1367-5931(02)00359-9. URL: http://www.sciencedirect.com/science/article/pii/S1367593102003599.

[13] B.W. Van De Waal. In: *Chemical Physics Letters* 123.1 (1986), pp. 69–72. ISSN: 0009-2614. DOI: https://doi.org/10.1016/0009-2614(86)87017-8. URL: http://www.sciencedirect.com/science/article/pii/0009261486870178.

[14] M. Samy El-Shall, George M. Daly, and Douglas Wright. "Experimental and theoretical study of benzene (acetonitrile)n clusters, n=1–4". In: *The Journal of Chemical Physics* 116.23 (2002), pp. 10253–10266. DOI: 10.1063/1.1476317. eprint: https://doi.org/10.1063/1.1476317. URL: https://doi.org/10.1063/1.1476317.

[15] Pavel Hobza, Heinrich L. Selzle, and Edward W. Schlag. "Potential Energy Surface of the Benzene Dimer: Ab Initio Theoretical Study". In: *Journal of the American Chemical Society* 116.8 (1994), pp. 3500–3506. DOI: 10.1021/ja00087a041. eprint: https://doi.org/10.1021/ja00087a041. URL: https://doi.org/10.1021/ja00087a041.

[16] Susil Silva and John D. Head. "A theoretical investigation of the aluminum-benzene complex". In: *Journal of The American Chemical Society - J AM CHEM SOC* 114 (July 1992). DOI: 10.1021/ja00042a029.

[17] Denis E. Bergeron et al. "Formation of Al13I-: Evidence for the Superhalogen Character of Al13". In: *Science* 304.5667 (2004), pp. 84–87. ISSN: 0036-8075. DOI: 10.1126/science.1093902. eprint: https://science.sciencemag.org/content/304/5667/84.full.pdf. URL: https://science.sciencemag.org/content/304/5667/84.

[18] Christopher A. Hunter and Jeremy K. M. Sanders. "The nature of .pi.-.pi. interactions". In: *Journal of the American Chemical Society* 112.14 (1990), pp. 5525–5534. DOI: 10.1021/ja00170a016. eprint: https://doi.org/10.1021/ja00170a016. URL: https://doi.org/10.1021/ja00170a016.

[19] Eluvathingal D. Jemmis et al. "Bond length and bond multiplicity: -bond prevents short -bonds". In: *Chem. Commun.* (20 2006), pp. 2164–2166. DOI: 10.1039/B602116F. URL: http://dx.doi.org/10.1039/B602116F.

[20] "Photoelectron spectra of aluminum cluster anions: Temperature effects and ab initio simulations". In: *Physical Review B* 60 (Sept. 1999). DOI: 10.1103/PhysRevB.60.R11297.

[21] "New structure for the most stable isomer of the benzene dimer: A quantum chemical study". In: *The Journal of Physical Chemistry* 97 (Apr. 1993). DOI: 10.1021/j100118a002.

[22] "A theoretical investigation of the aluminum-benzene complex". In: *Journal of The American Chemical Society - J AM CHEM SOC* 114 (July 1992). DOI: 10.1021/ja00042a029.

[23] "Magnetism of small vanadium clusters". In: *Nanostructured Materials* 3 (May 1991), pp. 331–335. DOI: 10.1016/0965-9773(93)90095-S.

[24] "A bird's-eye view of density-functional theory". In: *Braz. J. Phys.* 36 (Dec. 2002). DOI: 10.1590/S0103-97332006000700035.

[25] Jeremiah A. Marsden, Matthew J. O'Conno, and Michael M. Haley. "Synthesis and Characterization of Multiply Fused Dehydrobenzoannulenoannulene Topologies". In: *Organic Letters* 6.14 (2004). PMID: 15228285, pp. 2385–2388. DOI: 10.1021/ol049227f. eprint: https://doi.org/10.1021/ol049227f. URL: https://doi.org/10.1021/ol049227f.

[26] "Exploiting non-covalent π interactions for catalyst design". In: *Nature* 543 (Mar. 2017), pp. 637–646. DOI: 10.1038/nature21701.

[27] O. V. Gritsenko et al. "Comparison of the Accurate KohnSham Solution with the Generalized Gradient Approximations (GGAs) for the SN2 Reaction F- + CH3F FCH3 + F-: A Qualitative Rule To Predict Success or Failure of GGAs". In: *The Journal of Physical Chemistry A* 104.37 (2000), pp. 8558–8565. DOI: 10.1021/jp001061m. eprint: https://doi.org/10.1021/jp001061m. URL: https://doi.org/10.1021/jp001061m.

[28] "The role of non-covalent interactions in electrocatalytic fuel-cell reactions on platinum". In: *Nature chemistry* 1 (Sept. 2009), pp. 466–72. DOI: 10.1038/nchem.330.

[29] G. te Velde et al. “Chemistry with ADF”. In: *J. Comput. Chem.* 22.9 (2001), pp. 931–967. ISSN: 1096-987X. DOI: 10.1002/jcc.1056. URL: http://dx.doi.org/10.1002/jcc.1056.

[30] C. Fonseca Guerra et al. “Towards an order-N DFT method”. In: *Theoretical Chemistry Accounts* 99.6 (Nov. 1998), pp. 391–403. ISSN: 1432-2234. DOI: 10.1007/s002140050353. URL: https://doi.org/10.1007/s002140050353.

[31] John P. Perdew, Kieron Burke, and Matthias Ernzerhof. “Generalized Gradient Approximation Made Simple”. In: *Phys. Rev. Lett.* 77 (18 Oct. 1996), pp. 3865–3868. DOI: 10.1103/PhysRevLett.77.3865. URL: https://link.aps.org/doi/10.1103/PhysRevLett.77.3865.

[32] Stefan Grimme et al. “A consistent and accurate ab initio parametrization of density functional dispersion correction (DFT-D) for the 94 elements H-Pu”. In: *The Journal of Chemical Physics* 132.15 (2010), p. 154104. DOI: 10.1063/1.3382344. URL: https://doi.org/10.1063/1.3382344.

[33] Stefan Grimme, Stephan Ehrlich, and Lars Goerigk. “Effect of the damping function in dispersion corrected density functional theory”. In: *Journal of Computational Chemistry* 32.7 (), pp. 1456–1465. DOI: 10.1002/jcc.21759. eprint: https://onlinelibrary.wiley.com/doi/pdf/10.1002/jcc.21759. URL: https://onlinelibrary.wiley.com/doi/abs/10.1002/jcc.21759.

[34] E. Van Lenthe and E. J. Baerends. “Optimized Slater-type basis sets for the elements 1–118”. In: *Journal of Computational Chemistry* 24.9 (2003), pp. 1142–1156. DOI: 10.1002/jcc.10255. eprint: https://onlinelibrary.wiley.com/doi/pdf/10.1002/jcc.10255. URL: https://onlinelibrary.wiley.com/doi/abs/10.1002/jcc.10255.

[35] E. van Lenthe, E. J. Baerends, and J. G. Snijders. “Relativistic regular two-component Hamiltonians”. In: *The Journal of Chemical Physics* 99.6 (1993), pp. 4597–4610. DOI: 10.1063/1.466059. eprint: https://doi.org/10.1063/1.466059. URL: https://doi.org/10.1063/1.466059.

[36] E. van Lenthe, E. J. Baerends, and J. G. Snijders. “Relativistic total energy using regular approximations”. In: *The Journal of Chemical Physics* 101.11 (1994), pp. 9783–9792. DOI: 10.1063/1.467943. eprint: https://doi.org/10.1063/1.467943. URL: https://doi.org/10.1063/1.467943.

[37] Erik van Lenthe, Andreas Ehlers, and Evert-Jan Baerends. “Geometry optimizations in the zero order regular approximation for relativistic effects”. In: *The Journal of Chemical Physics* 110.18 (1999), pp. 8943–8953. DOI: 10.1063/1.478813. eprint: https://doi.org/10.1063/1.478813. URL: https://doi.org/10.1063/1.478813.

[38] Evert Jan Baerends et al. *ADF2017, SCM, Theoretical Chemistry, Vrije Universiteit, Amsterdam, The Netherlands, https://www.scm.com.*